r-Process Nucleosynthesis in Shocked Surface Layers of O-Ne-Mg Cores

H. Ning and Y.-Z. Qian

School of Physics and Astronomy, University of Minnesota, Minneapolis, MN 55455

`hning@physics.umn.edu; qian@physics.umn.edu`

and

B. S. Meyer

Department of Physics and Astronomy, Clemson University, Clemson, SC 29634

`mbradle@clemson.edu`

ABSTRACT

We demonstrate that rapid expansion of the shocked surface layers of an O-Ne-Mg core following its collapse can result in r-process nucleosynthesis. As the supernova shock accelerates through these layers, it makes them expand so rapidly that free nucleons remain in disequilibrium with α-particles throughout most of the expansion. This allows heavy r-process isotopes including the actinides to form in spite of the very low initial neutron excess of the matter. We estimate that yields of heavy r-process nuclei from this site may be sufficient to explain the Galactic inventory of these isotopes.

Subject headings: nuclear reactions, nucleosynthesis, abundances — shock waves — supernovae: general

1. Introduction

In this Letter we propose a new astrophysical site for r-process nucleosynthesis. In particular, we show that heavy nuclei with mass numbers $A > 130$ through the actinides may be produced in the shocked surface layers of an O-Ne-Mg core following its gravitational collapse. Stellar evolution models show that stars of ~ 8–$11\,M_\odot$ develop degenerate O-Ne-Mg cores, at least some of which eventually collapse to produce supernovae (SNe; e.g., Nomoto 1984, 1987; Garcia-Berro & Iben 1994; Ritossa et al. 1996, 1999; Garcia-Berro et al.

1997; Iben et al. 1997; Poelarends et al. 2007). Such a core is separated from the hydrogen envelope by a thin C-O shell and an even thinner He shell. However, the density falls off so steeply in the region immediately above the core that we shall refer to the C-O and He shells as the surface layers of the core. These layers result from He and H burning coupled with convection during the pre-SN evolution, and this pre-supernova burning can give rise to a metallicity-independent neutron excess through reaction sequences such as $^{12}C(p, \gamma)^{13}N$ followed by β^+ decay of ^{13}N to ^{13}C (Nomoto 2007, personal communication). The SN shock rapidly accelerates as it propagates through the surface layers of the core. This gives rise to fast expansion of the shocked ejecta on timescales of $\sim 10^{-4}$ s. Together with an entropy of $S \sim 100$ (in units of Boltzmann's constant k per nucleon) and an initial electron fraction of $Y_e \sim 0.495$ (e.g., for a composition of $^{13}C : {}^{12}C : {}^{16}O \sim 1 : 3 : 3$ by mass), this fast expansion enables an r-process to occur in the shocked ejecta, producing neutron-rich nuclei with $A > 130$ through the actinides.

We discuss the conditions during the expansion of the shocked ejecta in §2. Nucleosynthesis calculations for two different initial compositions are presented in §3 with and without neutrino reactions on free nucleons and α-particles. We discuss the implications of this new r-process model for abundances in metal-poor stars and for general Galactic chemical evolution in §4.

2.   Conditions During Expansion of Shocked Surface Layers

In the generic scenario of stellar core collapse, the inner core becomes a proto-neutron star (PNS) and bounces on reaching supra-nuclear density. This launches a shock, which propagates into the still collapsing outer core and falters. According to the neutrino-driven SN mechanism (Bethe & Wilson 1985), the shock is re-energized through heating of the material behind it by the neutrinos emitted from the PNS. Using Nomoto's (1984, 1987) model for a $1.38 \, M_\odot$ O-Ne-Mg core, Mayle & Wilson (1988), and most recently, Kitaura et al. (2006) (see also Janka et al. 2007) indeed obtained neutrino-driven explosion although with very different final explosion energies. For our purpose, the exact explosion energy does not matter so long as the re-energized shock propagates through the surface layers of the core with a sufficient speed. As only stars in a very narrow range of ~ 8–$11 \, M_\odot$ develop O-Ne-Mg cores, we consider Nomoto's (1984, 1987) $1.38 \, M_\odot$ core model, which was evolved from the He core of a $\approx 9 \, M_\odot$ progenitor, to be representative and adopt its quantitative description of the pre-SN conditions. In addition, we use the simulations of Mayle & Wilson (1988) and Kitaura et al. (2006) based on this model as a guide to the shock propagation.

At the onset of collapse, the core is surrounded by $\sim 0.1 \, M_\odot$ of C and O, which in turn is

surrounded by several $10^{-6}\,M_\odot$ of He. We are interested in the outer C-O layer that contains several $10^{-5}\,M_\odot$. This layer is located at radii $r \approx 10^8$ cm and has a thickness of $\approx 5 \times 10^6$ cm. The density ρ within this region changes from 10^6 to 10^5 g cm^{-3}. The steepness of this fall-off is measured by $w \equiv -d\ln\rho/d\ln r$, which is 61.7 at $\rho = 3 \times 10^5$ g cm^{-3}. This can be understood from the condition of hydrostatic equilibrium, $-(1/\rho)dP/dr = GM_C/r^2$, where G is the gravitational constant, $M_C = 1.38\,M_\odot$ is the core mass, and P is the pressure provided by electrons and nuclei with temperature $T \sim 6 \times 10^8$ K. The pre-SN density structure changes as a result of core collapse. However, the local free-fall timescale at $r \approx 10^8$ cm is $\sim \sqrt{r^3/(GM_C)} \sim 0.1$ s, comparable to the time between the onset of core collapse and shock arrival at this radius. To zeroth order, we assume that the pre-SN density structure in the region of interest remains unchanged before being shocked.

The SN simulations mentioned above showed that the shock speed in the region of interest is $v_{\rm sh} \sim 10^{10}$ cm s^{-1}. For such $v_{\rm sh}$, the strong shock condition $\rho v_{\rm sh}^2 \gg P$ is satisfied and the energy density of the shocked matter is expected to be dominated by the contributions from relativistic particles (radiation and electron-positron pairs). In this case, the density, velocity, and pressure of the shocked matter (with the subscript "p" standing for "post-shock") are given by (e.g., Chevalier 1976)

$$\rho_p = 7\rho, \ v_p = \frac{6}{7}v_{\rm sh}, \ P_p = \frac{6}{7}\rho v_{\rm sh}^2, \tag{1}$$

respectively. Using Eq. (1) and $P_p = (11/12)a_{\rm rad}T_p^4$ with $a_{\rm rad}$ being the radiation constant, we obtain the post-shock temperature

$$T_p = 1.05 \times 10^{10}\rho_6^{1/4}v_{\rm sh,10}^{1/2} \ {\rm K} \tag{2}$$

and the post-shock entropy in relativistic particles

$$S = \frac{11}{3}\frac{a_{\rm rad}T_p^3}{N_A\rho_p} = 56.1\frac{v_{\rm sh,10}^{3/2}}{\rho_6^{1/4}} \ k \ {\rm nucleon}^{-1}, \tag{3}$$

where ρ_6 is the pre-shock density in units of 10^6 g cm^{-3}, $v_{\rm sh,10}$ is the shock speed in units of 10^{10} cm s^{-1}, N_A is Avogadro's number. The entropy S is also a measure of the energy density in relativistic particles relative to that in nonrelativistic ones. Equation (3) gives $S \gg 1$ in the region of interest, so the corresponding energy density of the shocked matter is indeed dominated by relativistic particles.

Matzner & McKee (1999) showed that $v_{\rm sh}$ at a specific r depends on the pre-shock density at r and the amount of matter entrained by the shock prior to reaching r. As the region of interest is very thin and adds very little to the matter already entrained by the shock, we

expect that the shock speed in this region takes the form $v_{\rm sh} \propto \rho^{-0.19}$ (Matzner & McKee 1999), which gives

$$\frac{dv_{\rm sh}}{dr} = -0.19 \left(\frac{d\ln\rho}{d\ln r} \right) \frac{v_{\rm sh}}{r} = 0.19w \left(\frac{v_{\rm sh}}{r} \right). \tag{4}$$

We assume that matter moves with a constant velocity v_p after being shocked. Consider a mass element initially sandwiched between radii r and $r + \delta r$. When the matter at $r + \delta r$ is shocked, the matter initially at r has moved to $r + (v_p/v_{\rm sh})\delta r = r + (6/7)\delta r$. The reduction of the mass element's thickness from δr to $\delta r/7$ results in the factor of 7 increase in its post-shock density (see Eq. [1]). Subsequently, the matter at the inner and outer radii of the mass element move with velocities of v_p and $v_p + (dv_p/dr)\delta r$, respectively. It can be shown that the density $\tilde{\rho}$ of the shocked mass element evolves with time t as:

$$\tilde{\rho}(t) = \frac{\rho_p}{[1 + (t/\tau_1)]^2 [1 + (t/\tau_2)]}, \tag{5}$$

where $t = 0$ is the time at which the mass element is shocked, and

$$\tau_1 = \frac{r}{v_p}, \quad \tau_2 = \frac{1}{7(dv_p/dr)} = \frac{\tau_1}{1.33w}. \tag{6}$$

In the denominator of Eq. (5), the first factor accounts for the expansion of the surface area of the mass element and the second for the increase of its thickness. In relating τ_2 to τ_1 in Eq. (6), we have used Eqs. (1) and (4). To very good approximation, the expansion of the shocked mass element is adiabatic. This then specifies the time evolution of its temperature $\tilde{T}$ as

$$\tilde{T}(t) = \frac{T_p}{[1 + (t/\tau_1)]^{2/3} [1 + (t/\tau_2)]^{1/3}}. \tag{7}$$

Considering the proximity of the region of interest to the PNS, we also study how interaction with the intense neutrino flux affects nucleosynthesis. Due to the short timescales $\tau_1 \sim 10^{-2}$ s and $\tau_2 \sim 10^{-4}$ s for the expansion of a shocked mass element, the neutrino luminosity and energy spectra do not change during the expansion. We take the luminosity to be 4×10^{52} erg s^{-1} per neutrino species, $\langle E_\nu^2 \rangle / \langle E_\nu \rangle = 11$ and 16 MeV for ν_e and $\bar{\nu}_e$, respectively, and $\langle E_\nu \rangle = 25$ MeV for $\nu_x = \nu_\mu$, $\bar{\nu}_\mu$, ν_τ, $\bar{\nu}_\tau$, where $\langle E_\nu \rangle$ and $\langle E_\nu^2 \rangle$ are the averages of the neutrino energy and its square, respectively, over the relevant spectrum (the rates of interest for ν_e and $\bar{\nu}_e$ are essentially determined by the values of $\langle E_\nu^2 \rangle / \langle E_\nu \rangle$ for these species and insensitive to their detailed spectra, while the rates of interest for ν_x assume a black-body-like spectrum with a temperature of 8 MeV). We include the reactions $\nu_e + n \to p + e^-$, $\bar{\nu}_e + p \to n + e^+$, $\nu_x + {}^4{\rm He} \to {}^3{\rm He} + n$, and $\nu_x + {}^4{\rm He} \to {}^3{\rm H} + p$, the rates of which are 0.253, 0.250, 1.28×10^{-2}, and 1.40×10^{-2} s^{-1} per target, respectively, at a

radius of 10^8 cm (Qian & Woosley 1996; Woosley et al. 1990). For a mass element initially at radius r, its radius $\tilde{r}$ evolves as

$$\tilde{r}(t) = r[1 + (t/\tau_1)]. \qquad (8)$$

All the neutrino reaction rates for this mass element scale as $[\tilde{r}(t)]^{-2}$.

3. Nucleosynthesis in Shocked Ejecta

We focus on a specific mass element initially at $r = 10^8$ cm. The pre-shock density structure at this position is characterized by $\rho_6 = 0.3$ and $w = 61.7$. We take $v_{\text{sh},10} = 1.5$ at this position, which gives $T_p = 9.52 \times 10^9$ K, $\tau_1 = 7.8 \times 10^{-3}$ s, and $\tau_2 = 9.48 \times 10^{-5}$ s. The postshock density is $\rho_p = 2.1 \times 10^6$ g cm^{-3}, corresponding to an entropy of $S = 139$. We study the nucleosynthesis during the expansion of the above mass element for two different initial compositions: (1) $X(^{12}\text{C}) = X(^{16}\text{O}) = 0.5$ corresponding to $Y_e = 0.5$ as in Nomoto's (1984, 1987) original model, and (2) $X(^{13}\text{C}) = 0.14$, $X(^{12}\text{C}) = X(^{16}\text{O}) = 0.43$ corresponding to $Y_e = 0.495$, which allows for possible production of ^{13}C due to mixing during the pre-SN evolution. Here, for example, $X(^{12}\text{C})$ is the mass fraction of ^{12}C. The above two cases are referred to as trajectories 1 and 2 when neutrino reactions are not included and as trajectories $1'$ and $2'$ when these reactions are included.

To study the nucleosynthesis associated with trajectories 1 and 2, we use the Clemson nuclear reaction network (Jordan & Meyer 2004), which includes nuclear species from neutrons and protons through the actinides. Because the network flow reached the top of the reaction network in some cases, we included nuclear fission by allowing the most massive species in the network (^{276}U) to fission into two fragments (with $Z = 42$ and 50, respectively). This is a crude treatment that will require improvement in follow-up calculations. Nevertheless, it illustrates the effect of fission cycling.

Figure 1 shows the final abundances for trajectories 1 (top panel) and 2 (bottom panel) as a function of A. Trajectory 1 (initial $Y_e = 0.5$) makes heavy, neutron-rich nuclei, although the abundance pattern does not resemble the solar r-process abundance distribution well. Trajectory 2 (with initial $Y_e = 0.495$) makes heavy, neutron-rich nuclei, including actinides, and the resulting abundance pattern shows three distinct peaks in rough agreement with the solar r-process distribution. The peaks made by trajectory 2 lie several mass units above the corresponding solar r-process abundance peaks. This is mainly due to the rather extensive exposure to neutron capture for this trajectory: there are still about 15 free neutrons per heavy nucleus at the end of the run. The reason why trajectories 1 and 2 are able to produce heavy, neutron-rich nuclei despite the zero to low initial neutron excess is the persistent

nucleon–α-particle disequilibrium discussed by Meyer (2002). In these expansions, the initial distribution of nuclei is quickly broken down into nuclear statistical equilibrium, which is dominated by free neutrons and protons. As the material expands and cools, the free nucleons assemble into α-particles and heavier nuclei. Because of the rapidness of the expansion, however, the free nucleons do not assemble into heavier species (particularly α-particles) as quickly as equilibrium demands. This leaves a large excess of these free nucleons, which push the heavy nuclei to very high mass. For example, for trajectory 2, at $T_9 \approx 4$, the abundance distribution is dominated by free neutrons and protons, α-particles, and nuclei with mass number $A \approx 140$. Specifically, the mass fractions of free neutrons and protons, α-particles, and heavy nuclei at this temperature are $\approx 1.3\%$, 0.3%, 97.6%, and 0.6%, respectively. The heavy nuclei serve as the seeds for the subsequent r-process nucleosynthesis.

We expect that the final abundance distribution will depend on the details of the trajectories of the mass elements at late times. Indeed, we note that for trajectory 2, expansion occurs so rapidly that reaction freezeout occurs because the density drops to such a low value that neutron-capture timescales become long, not because the neutrons are all consumed. The result is that there are still about 15 free neutrons per heavy nucleus at the end of the run (the final mass fractions of free neutrons, α-particles, and heavy nuclei are $\approx 0.2\%$, 98%, and 2%, respectively). We confirmed this by running a calculation identical to trajectory 2 except that the expansion slowed at late times and allowed the neutrons to be all consumed. The resulting pattern was broadly similar to that in the lower panel of Fig. 1, but the contrast between the peaks and valleys was smaller.

We also followed trajectories 1′ and 2′, which were identical to trajectories 1 and 2 except that neutrino reactions were included. The neutrino interactions had negligible effects on the abundance patterns. This is because expansion carried the material away so rapidly that the total number of neutrino interactions per nucleon or nucleus was $\ll 1$ during the expansion.

4. Discussion and Conclusions

We have proposed a new model of r-process nucleosynthesis in O-Ne-Mg-core collapse SNe. Unlike previous models based on assumed extremely neutron-rich ejecta (e.g., Wheeler et al. 1998; Wanajo et al. 2003), our model relies on the fast expansion of the shocked matter in the weakly neutron-rich surface layers of an O-Ne-Mg core to achieve a disequilibrium between free nucleons, α-particles, and heavier nuclei. As shown by Meyer (2002), the significant presence of free nucleons in disequilibrium facilitates the production of seed nuclei with $A \sim 140$ during the expansion. For matter with an initial $Y_e = 0.495$, the

neutron excess is sufficient for an r-process with fission cycling to occur, producing dominantly the nuclei with $A > 130$ through the actinides. The key to the fast expansion of the shocked matter is the steep density gradient in the surface layers of an O-Ne-Mg core, which enables the inner and outer surfaces of a mass element to expand with significantly different velocities, thus making its density drop much faster.

O-Ne-Mg-core collapse SNe were also proposed as the source for the heavy r-process elements (r-elements) with $A > 130$ (Ba and higher atomic numbers) based on considerations of Galactic chemical evolution (e.g., Mathews et al. 1992; Ishimaru & Wanajo 1999). A strong argument for this proposal was presented using observations of metal-poor stars (Qian & Wasserburg 2002, 2003). In addition, the key issues regarding the sources for the r-elements based on observations and basic understanding of stellar models were summarized in Qian & Wasserburg (2007). Data on the metal-poor stars CS 31082–001 (Hill et al. 2002), HD 115444, and HD 122563 (Westin et al. 2000) show that their abundances of the heavy r-elements differ by a factor up to $\sim 10^2$. In contrast, these stars have essentially the same abundances of the elements between O and Ge (e.g., [Fe/H] $\equiv \log(\text{Fe/H}) - \log(\text{Fe/H})_\odot \sim -3$). Furthermore, when CS 22892–052 ([Fe/H] $= -3.1$, Sneden et al. 2003) is compared with HD 221170 ([Fe/H] $= -2.2$, Ivans et al. 2006) and CS 31082–001 ([Fe/H] $= -2.9$) with BD $+17°3248$ ([Fe/H] $= -2.1$, Cowan et al. 2002), data show that the stars in either pair have nearly the same abundances of heavy r-elements but the abundances of the elements between O and Ge differ by a factor of ~ 8 and 6 for the former and latter pair, respectively. These results appear to require that the production of the heavy r-elements be decoupled from that of the elements between O and Ge (Qian & Wasserburg 2002, 2003, 2007). As Fe-core collapse SNe from progenitors of $> 11\,M_\odot$ are the major source for the latter group of elements at low metallicities, this strongly suggests that such SNe are not the source for the heavy r-elements. The elements between O and Ge are produced between the core and the H envelope by explosive burning during a core-collapse SN or by hydrostatic burning during its pre-SN evolution. Models of O-Ne-Mg-core collapse SNe show that the total amount of material ejected from between the core and the H envelope is only ~ 0.01–$0.04\,M_\odot$ (Mayle & Wilson 1988; Kitaura et al. 2006), much smaller than the $\sim 1\,M_\odot$ for Fe-core collapse SNe. Thus, O-Ne-Mg-core collapse SNe contribute very little to the elements between O and Ge. The decoupling between these elements and the heavy r-elements can then be explained by attributing the heavy r-elements to such SNe as argued in Qian & Wasserburg (2002, 2003, 2007). This attribution is supported by the r-process model proposed here.

The collapse of O-Ne-Mg cores may comprise up to $\sim 20\%$ of all core-collapse events and may thus occur roughly once a century (e.g., Poelarends et al. 2007). Assume that this frequency of occurrence is associated with a reference gas of $\sim 10^{10}\,M_\odot$ and that the O-Ne-Mg-core collapse SNe over the Galactic history of $\sim 10^{10}$ yr enriched this gas with a

solar mass fraction of $\sim 4 \times 10^{-8}$ of heavy r-elements. We find that each SN must produce $\sim 4 \times 10^{-6}\, M_\odot$ of heavy r-elements. The total mass fraction of heavy r-elements produced during the expansion associated with trajectory 2 is ~ 0.02 and a total $\sim 3 \times 10^{-5}\, M_\odot$ of ejecta may experience such expansion in Nomoto's (1984, 1987) O-Ne-Mg core model. This assumes an initial composition with $Y_e = 0.495$ and would give $\sim 6 \times 10^{-7}\, M_\odot$ of heavy r-elements per SN. A slightly smaller $Y_e = 0.49$ would double the initial neutron excess and the final r-process production, giving $\sim 10^{-6}\, M_\odot$ of heavy r-elements. Thus, we consider the model proposed here has the potential to account for the Galactic inventory of such elements. To further test this model, we urge two lines of important studies: (1) calculating the evolution of ~ 8–$11\, M_\odot$ stars to determine the pre-SN conditions of O-Ne-Mg cores, especially the neutron excess and density structure of the surface layers; and (2) simulating the collapse of such cores and the subsequent shock propagation to determine the conditions of the shocked surface layers. As these layers contain very little mass, simulations with extremely fine mass resolutions are required to demonstrate the fast expansion of shocked ejecta that is proposed here as the key to the production of heavy r-elements. The pre-SN abundance of ^{13}C in the surface layers also requires investigation as this appears critical to the total yields of heavy r-elements.

REFERENCES

Bethe, H. A. & Wilson, J. R. 1985, ApJ, 295, 14

Chevalier, R. A. 1976, ApJ, 207, 872

Cowan, J. J., Sneden, C., Burles, S., Ivans, I. I., Beers, T. C., Truran, J. W., Lawler, J. E., Primas, F., Fuller, G. M., Pfeiffer, B., & Kratz, K.-L. 2002, ApJ, 572, 861

Garcia-Berro, E. & Iben, I. 1994, ApJ, 434, 306

Garcia-Berro, E., Ritossa, C., & Iben, I. J. 1997, ApJ, 485, 765

Hill, V., Plez, B., Cayrel, R., Beers, T. C., Nordström, B., Andersen, J., Spite, M., Spite, F., Barbuy, B., Bonifacio, P., Depagne, E., François, P., & Primas, F. 2002, A&A, 387, 560

Iben, I. J., Ritossa, C., & Garcia-Berro, E. 1997, ApJ, 489, 772

Ishimaru, Y. & Wanajo, S. 1999, ApJ, 511, L33

Ivans, I. I., Simmerer, J., Sneden, C., Lawler, J. E., Cowan, J. J., Gallino, R., & Bisterzo, S. 2006, ApJ, 645, 613

Janka, H.-T., Marek, A., & Kitaura, F.-S. 2007, ArXiv e-prints, 706

Jordan, IV, G. C. & Meyer, B. S. 2004, ApJ, 617, L131

Kappeler, F., Beer, H., & Wisshak, K. 1989, Reports of Progress in Physics, 52, 945

Kitaura, F. S., Janka, H.-T., & Hillebrandt, W. 2006, A&A, 450, 345

Mathews, G. J., Bazan, G., & Cowan, J. J. 1992, ApJ, 391, 719

Matzner, C. D. & McKee, C. F. 1999, ApJ, 510, 379

Mayle, R. & Wilson, J. R. 1988, ApJ, 334, 909

Meyer, B. S. 2002, Physical Review Letters, 89, 231101

Nomoto, K. 1984, ApJ, 277, 791

—. 1987, ApJ, 322, 206

Poelarends, A. J. T., Herwig, F., Langer, N., & Heger, A. 2007, ArXiv e-prints, 705

Qian, Y.-Z. & Wasserburg, G. J. 2002, ApJ, 567, 515

—. 2003, ApJ, 588, 1099

—. 2007, Phys. Rep., 442, 237

Qian, Y.-Z. & Woosley, S. E. 1996, ApJ, 471, 331

Ritossa, C., Garcia-Berro, E., & Iben, I. J. 1996, ApJ, 460, 489

Ritossa, C., García-Berro, E., & Iben, I. J. 1999, ApJ, 515, 381

Sneden, C., Cowan, J. J., Lawler, J. E., Ivans, I. I., Burles, S., Beers, T. C., Primas, F., Hill, V., Truran, J. W., Fuller, G. M., Pfeiffer, B., & Kratz, K.-L. 2003, ApJ, 591, 936

Wanajo, S., Tamamura, M., Itoh, N., Nomoto, K., Ishimaru, Y., Beers, T. C., & Nozawa, S. 2003, ApJ, 593, 968

Westin, J., Sneden, C., Gustafsson, B., & Cowan, J. J. 2000, ApJ, 530, 783

Wheeler, J. C., Cowan, J. J., & Hillebrandt, W. 1998, ApJ, 493, L101+

Woosley, S. E., Hartmann, D. H., Hoffman, R. D., & Haxton, W. C. 1990, ApJ, 356, 272
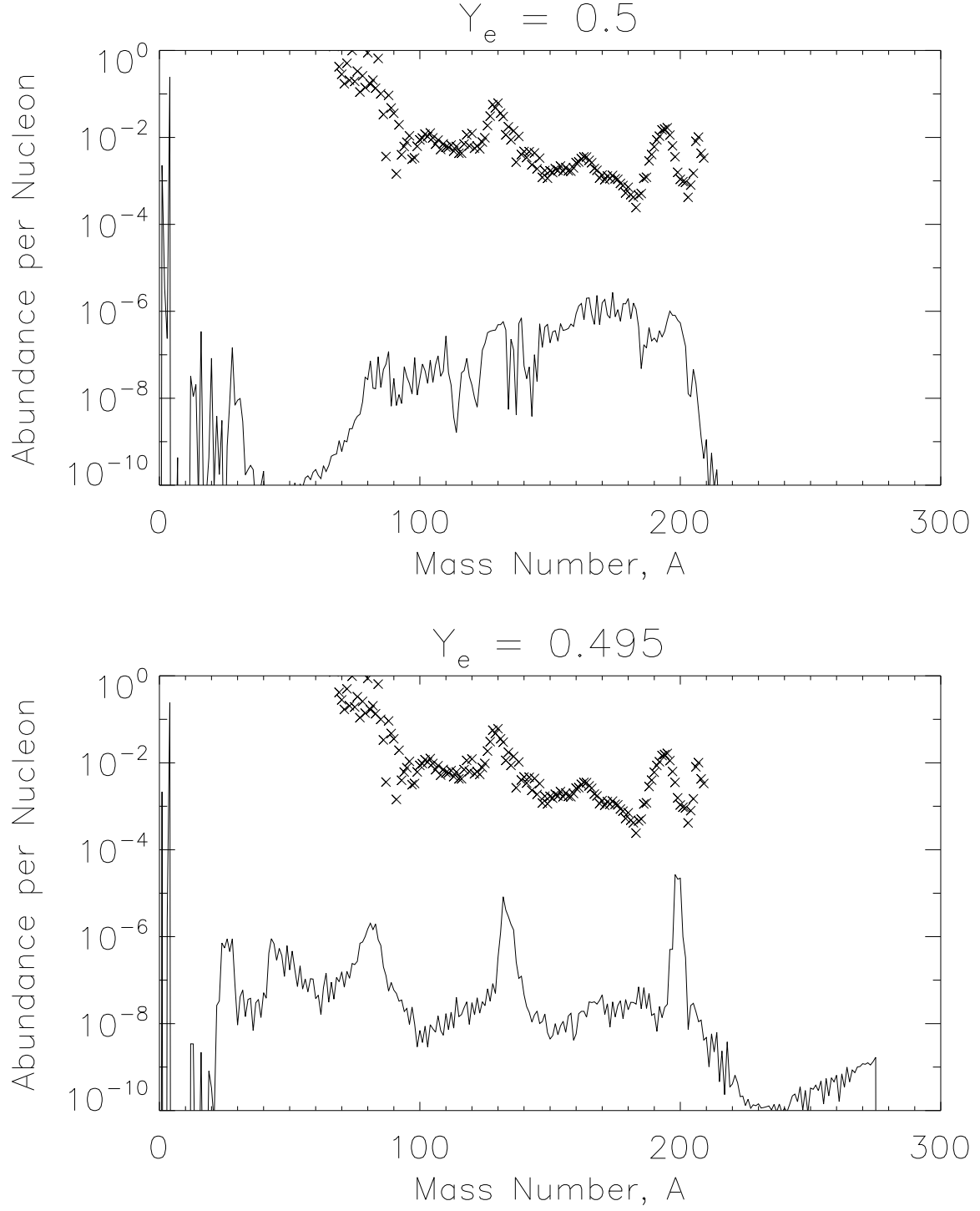
Fig. 1.— Final abundances versus mass number for trajectories 1 (top panel) and 2 (bottom panel). The (arbitrarily scaled) solar r-process abundances (Kappeler et al. 1989) are shown as ×'s for comparison. The final mass fractions resulting from both trajectories are $\approx 98\%$ α-particles and $\approx 2\%$ heavy nuclei.